Mathematical model of blood flow in a coronary capillary

G. FIBICH, Y. LANIR, AND N. LIRON
Department of Mathematics and Cardiac System Research Center, Department of Biomedical Engineering, Technion, Israel Institute of Technology, Haifa 32000, Israel

Fibich, G., Y. Lanir, and N. Liron. Mathematical model of blood flow in a coronary capillary. *Am. J. Physiol.* 265 (*Heart Circ. Physiol.* 34): H1829–H1840, 1993.—The coronary capillary flow is analyzed theoretically based on continuum mechanics. The capillary is a long, elastic, and permeable vessel loaded externally by tissue pressure, and it is subject to possible periodic length changes, together with adjacent myocytes. Capillary flow is driven by arteriolar-venular pressure difference. Ultrafiltration due to transmural hydrostatic and osmotic gradients is included, and consideration of mass conservation leads to a nonlinear flow equation. The results show that under physiological conditions ultrafiltration is of minor importance, and the analysis predicts regional differences in capillary flow. In regions with high tissue pressure (subendocardium), capillaries undergo significant periodic volume changes, giving rise to intramyocardial pumping. In those regions, capillary wall elasticity is of major importance. In regions with low tissue pressure (subepicardium), the possible periodic capillary length changes are predominant. The predicted flow patterns are in good qualitative agreement with measured epicardial phasic flow. In conclusion, the methodological advantage of a distributive analysis is demonstrated by its ability to elucidate and evaluate the role of flow determinants and their complex interactions.

coronary circulation; capillary flow; distributive analysis

CORONARY CIRCULATION has several unique features. Among them are the phasic nature of the arterial inflow and the venous return (12), the occurrence of retrograde flow, pronounced regional perfusion differences, the existence of a significant vascular compliance (20), the vanishing of flow at pressures lower than the zero-flow pressure, and the considerable autoregulatory capacity demonstrated by the coronary reserve (19).

It was estimated that more than half of both the total coronary volume and the vascular compliance resides in capillaries and venules (36), whereas arterioles are the major resistive component (23). Based on this information, it has been suggested that the microcirculation has a significant effect on the overall coronary flow. This influence is, however, not well understood. It is not known, for example, to what extent phenomena such as arterial retrograde flow and regional perfusion differences originate in the microcirculatory level. Even the relative importance of the various mechanisms that influence flow in the coronary microcirculation is not known.

This gap in knowledge and understanding stems mainly from difficulties in measuring blood velocities and pressures in the microvessels of the beating heart, especially in the inner layers. Direct microcirculatory measurements were carried out in the subepicardium (1, 11, 38, 39).

In the absence of direct measurements, analytic models can provide insight into the system and give answers to some of the above questions. Of the previously published models, most analyzed the dynamics of the coronary circulation by considering different levels of the vasculature (arteries, capillaries, and veins) as lumped components. Each component is represented by integral characteristics, such as resistance and compliance. The complex coronary circulation is represented by an electric or other circuit analog (see review of earlier works in Ref. 5). The effects of the flow-controlling mechanisms were introduced by considering mechanisms such as a vasculature waterfall (14), the intramyocardial pump (36), a combination of the two (e.g., 24), and the time-varying vascular elastance (25).

There is no general agreement as to the validity and significance of these proposed mechanisms. Moreover, the assumption that the flow can be adequately modeled by a lumped model has not been verified. Insight into these problems might be gained by a detailed analysis based on the fundamental laws of mechanics, which consider the distributive nature of the system.

With the adoption of this methodology in the present study, a model for the flow in a single coronary capillary is formulated based on the equations of flow and on the material properties of the capillaries. The capillary is modeled as a long elastic permeable tube. It is subjected to external loading of the interstitial fluid and myocardial fibers, whereas the pressures at the capillary ends vary with the cardiac cycle. The observations of Borg and Caulfield (6) on the effect of the collagen matrix on the capillary area lead to the hypothesis that capillaries may undergo length changes during the cardiac cycle, together with the myocytes to which they are attached. Indeed, capillary length changes have been reported in the myocardium (30).

The present study focuses attention on the capillary level, since capillaries occupy a major portion of the microvasculature volume (26) and ~30% of the total coronary volume, the largest fraction for a single compartment (36). Thus the characteristics of the capillary flow are expected to make a large contribution to the overall flow. The modeling process presented here can be used quite similarly for other coronary microvessels, using the appropriate structural and material data.

To the best of our knowledge, the only previous distributive model for coronary capillaries was developed

by Dinnar (13), who examined the effect of varying tissue pressure and ultrafiltration in a rigid capillary. Schmid-Schönbein et al. (32) modeled the blood flow in a skeletal muscle capillary, and they considered the viscoelastic properties of the capillaries. Chadwick et al. (10) developed a model for the entire coronary microcirculation, which began as a distributive model, by applying mechanical laws for the vessels and fluid. These were then reduced to a lumped model by a process of spatial averaging.

METHODS

Coronary capillary mechanics and kinematics. The distensibility of coronary capillaries is clearly demonstrated by the observation that they are narrower in systole than in diastole (26, 38). Detailed distensibility measurements were carried out for capillaries in the mesentery (2, 34) and in the spinotrapezius muscle (33). In these studies it was found that capillary distensibility was markedly nonlinear and viscoelastic in response to a sudden pressure increase. At low pressures, skeletal muscle capillaries appeared to be 40% stiffer than the mesenteric capillaries (33). Because there are no direct data on coronary capillaries, the present study will rely on the viscoelastic model of Skalak and Schmid-Schönbein (33). They showed that the time constant of the viscous behavior of the capillary wall is ~100 s. Therefore, for short times typical of the cardiac cycle (0–1 s), the wall response can be approximated as elastic. In the above study, pressure changes were found to be linearly related to the strain, so that

$$\Delta P = \alpha E \tag{1}$$

where $\Delta P = P(z,t) - P_T(t)$ is the local transmural pressure difference (the difference between the hydrostatic pressure in the capillary P and the external loading represented by an intramyocardial tissue pressure P_T), t is the time and E is the strain measure defined as

$$E = \frac{1}{2}\left\{\left[\frac{a(z,t)}{a_0}\right]^2 - 1\right\} \tag{2}$$

where $a(z,t)$ is the capillary radius, a_0 is the reference radius under zero transmural pressure ($\Delta P = 0$), and α is an elasticity coefficient. The measured value of α was in the range of 1,250 ± 450 mmHg for the instantaneous elastic response (33; see also *Values of parameters*).

A mechanism that did not receive attention in previous models is the possible periodic length change of a coronary capillary. A coronary capillary runs parallel to the adjacent myocytes (4) to which it is connected by a network of stiff and short collagen struts (8). These observations lead intuitively to the possibility that the capillary changes its length in accordance with the neighboring myocytes to which it is connected. Such length changes have been reported in skeletal muscle. Ellis et al. (15) found that in the extensor digitorum muscle of a rat, lengthening of the muscle fibers resulted in stretching of the capillaries and in a reduction of their tortuosity. Based on morphometric data, Poole et al. (30) concluded that in the myocardium, capillary length increases with increasing sarcomere length above 1.9 μm and decreases at short myocardial fiber length. This decrease is accompanied by little change in capillary tortuosity. Tortuosity was found to have only a small effect on the resistance to flow (9). In the present study attention is focused on the effects of the capillary length changes on the flow.

Because there are not sufficient quantitative data on the dynamic length change of coronary capillaries, the present study will consider the two opposite cases: one case with capillary length changes following that of the neighboring muscle fibers, and a second case of fixed capillary length.

In the first case, the capillary length-change hypothesis is expressed by

$$L(t) = \omega(t) L_0 \tag{3}$$

where $L(t)$ is the time-dependent capillary length, L_0 is the capillary length in the stress-free configuration, and $\omega(t)$ is the relative length change of the adjacent myocytes. In the second case we simply take $\omega(t) \equiv 1$.

We shall use a cylindrical coordinate system (r, θ, z) where the coordinate z runs along the capillary axis, r is the radial coordinate, and θ is the angular one. Radial symmetry is assumed throughout the model (e.g., no dependence on θ). The arterial end of the capillary is set at $z = 0$. The position of the venular end at time t is $L(t)$. We define $U(z, t)$ as the axial velocity of the capillary wall. It follows that

$$U(0, t) = 0; \qquad U[L(t), t] = L'(t) \tag{4}$$

where prime refers to the first time derivative.

With the assumption that the length changes of the capillary are uniform (all portions of the capillary experience the same length change), it follows that

$$U(z, t) = \frac{z}{L(t)} L'(t) = z\frac{\omega'(t)}{\omega(t)} \tag{5}$$

Fluid kinematics. The blood is a nonhomogeneous non-Newtonian fluid. Nevertheless, Lipowsky et al. (27) have shown that the specific resistance to blood flow in the microcirculation is inversely proportional to the fourth power of the vessel diameter, as in Poiseuille flow. The discharge (for a fixed length microvessel) is thus given by

$$Q = -\frac{\pi a^4}{8\mu} P_z \tag{6}$$

where μ represents the effective blood viscosity, and the z subscript denotes partial differentiation with respect to z.

Near the capillary wall, the fluid velocity is equal to the $U(z,t)$ (the no-slip condition). Hence, the capillary discharge is augmented by $\pi a^2 U$. It follows that the total capillary discharge is

$$Q = \pi a^2(z, t) U(z, t) + (-P_z)\frac{\pi a^4(z, t)}{8\mu} \tag{7}$$

Fluid exchange across the capillary wall follows Starling's Law

$$q = k(\Delta P - \Delta \Pi) \tag{8}$$

where q is the outward fluid flux per unit area, k is the filtration coefficient, and $\Delta\Pi$ is the colloid osmotic pressure difference between the plasma and the interstitial fluid.

By following the study of Schmid-Schönbein et al. (32), we expressed the conservation of mass for a distensible, permeable segment of the capillary vessel filled with incompressible blood as

$$\frac{\partial}{\partial t}[\pi a^2(z, t)] = -\frac{\partial}{\partial z} Q(z, t) - 2\pi a(z, t) q(z, t) \tag{9}$$

The normalized radius h is defined as

$$h(z, t) = \frac{a(z, t)}{a_0} \tag{10}$$

From *Eqs. 1* and *2* it follows that h^2 can be viewed as a nondi-

mensionalized pressure

$$h^2 = 1 + \frac{2\Delta P}{\alpha} \tag{11}$$

The P_T varies from endocardium to epicardium. Coronary capillaries run parallel to the myocytes, which are in turn approximately parallel to both the endocardial and epicardial surfaces. Hence, it is highly likely that P_T does not change along a single capillary. This is expressed by the equation

$$\frac{\partial}{\partial z} P_T \equiv 0 \tag{12}$$

It follows from *Eqs. 11, 12*, and the definition of ΔP, that

$$\frac{\partial}{\partial z} P = \frac{\partial}{\partial z} \Delta P = \frac{\alpha}{2} \cdot \frac{\partial}{\partial z} (h^2) \tag{13}$$

Thus, from *Eqs. 1, 5, 7*, and *13*

$$Q = \pi a_0^2 h^2 z \frac{\omega'(t)}{\omega(t)} - \frac{\pi a_0^4 \alpha}{48\mu} \cdot \frac{\partial}{\partial z} (h^6) \tag{14}$$

Substitution of *Eqs. 8, 10, 14*, in *Eq. 9* gives

$$\pi a_0^2 \frac{\partial}{\partial t} (h^2) = \frac{\pi a_0^4 \alpha}{48\mu} \cdot \frac{\partial^2}{\partial z^2} (h^6) - \pi a_0^2 \frac{\omega'(t)}{\omega(t)} \cdot \frac{\partial}{\partial z} (zh^2) - 2\pi a_0 k \left[\frac{\alpha}{2} h^3 - \left(\frac{\alpha}{2} + \Delta\Pi \right) h \right] \tag{15}$$

We introduce two nondimensional variables

$$\tau = t/T_0; \qquad \zeta = z/L(t) \tag{16}$$

into *Eq. 15*, where τ is a time variable, ζ is a normalized axial position variable, and T_0 is the time of one cardiac cycle. To keep notations simple, we use the same customary symbols for the nondimensional-dependent variables. By dividing the resulting equation by $\pi a_0^2/T_0$, we get

$$(h^2)_\tau = \frac{\beta}{\omega^2(\tau)} (h^6)_{\zeta\zeta} - \frac{\omega'(\tau)}{\omega(\tau)} h^2 - \lambda h^3 + (\lambda + \eta) h \tag{17}$$

where subscripts denote partial differentiation with respect to the nondimensional variables, and the nondimensional parameters of the model β, λ and η are given by

$$\beta = \frac{a_0^2 \alpha T_0}{48\mu L_0^2}; \qquad \lambda = \frac{k\alpha T_0}{a_0}; \qquad \eta = \frac{2\Delta\Pi k T_0}{a_0} \tag{18}$$

Dividing *Eq. 17* by $2h$, we have

$$h_\tau = \frac{\beta}{\omega^2(\tau)} (3h^4 h_{\zeta\zeta} + 15h^3 h_\zeta^2) - \frac{\omega'(\tau)}{2\omega(\tau)} h - \frac{\lambda}{2} (h^2 - 1) + \frac{\eta}{2} \tag{19}$$

which is a nonlinear parabolic equation with time-periodic coefficients.

The boundary conditions are derived by using *Eq. 11*

$$h(0, \tau) = h_A(\tau) = \left\{ 1 + \frac{2}{\alpha} [P_A(\tau) - P_T(\tau)] \right\}^{1/2}$$
$$h(1, \tau) = h_V(\tau) = \left\{ 1 + \frac{2}{\alpha} [P_V(\tau) - P_T(\tau)] \right\}^{1/2} \tag{20}$$

where $P_A(\tau)$ and $P_V(\tau)$ are the fluid pressures in the arterial and venular ends of the capillary, respectively, and $h_A(\tau)$ and $h_V(\tau)$ are normalized radii in the arterial and venular ends of the capillary, respectively.

The solution $h(\zeta,\tau)$ of *Eq. 19* must satisfy a periodicity condition

$$h(\zeta, \tau) = h(\zeta, \tau + 1) \tag{21}$$

Equations 19-21 are the mathematical formulation of the model.

Value of parameters. Coronary capillary diameter was found to be 5-7 μm in humans (29) and 5.6 ± 1.3 μm (presumably at maximal dilatation) in dogs (3). Capillary length varies from 500 to 1,000 μm (3) in dogs. We shall, therefore, set $a_0 = 2.5$ μm and $L_0 = 750$ μm, where a_0 and L_0 are typical values of the reference radius and length, respectively. The cardiac period in a dog is taken as $T_0 = 0.5$ s.

In the present model, μ stands for the apparent (effective) viscosity of the blood, which depends on the microvessel radius, hematocrit, and shear rate. A typical value for small capillaries is $\mu = 5$ cP (27).

The value of the instantaneous elastic response of the capillary wall in the spinotrapezius muscle, as measured by Skalak and Schmid-Schönbein (33), is $\alpha = 1{,}250 \pm 450$ mmHg. In another study, which relates specifically to coronary vessels, Spaan (36) estimated the capillary distensibility to be around 5.5×10^{-3}/mmHg. This value corresponds to $\alpha = 364$ mmHg. Hence, we take $\alpha = 500$ mmHg as the typical value, but in the subsequent analysis and simulations the value of α will be varied between 200 and 1,250 mmHg. Dynamic autoregulatory mechanisms that may effect the wall distensibility are not considered, since the present analysis relates to a fixed level of the autoregulatory state corresponding to steady physiological cardiac output.

Filtration constants of capillaries were found to be $k = 0.68 \times 10^{-6}$ cm·s^{-1}·cmH_2O^{-1} for rat skeletal muscle (7). Smaje and Swayne (34) and Baldwin and Gore (2) showed that when interpreting experimental data to determine the filtration coefficient, the capillary distensibility has to be taken into account. As a result, the computed values of the filtration coefficient decrease considerably. Baldwin and Gore (2) obtained mean values of k as $0.61 \pm 0.12 \times 10^{-6}$ cm·s^{-1}·cmH_2O^{-1}. Smaje and Swayne (34) found that the large apparent gradient in k between the arteriolar and venular ends of rat intestinal muscle capillaries was significantly reduced when distensibility was taken into account. In the present study it will be assumed that k is constant along the capillary, and of typical value $k = 0.6 \times 10^{-6}$ cm·s^{-1}·cmH_2O^{-1}.

Values of colloid osmotic pressures are 25 mmHg for the plasma and 20-30 mmHg for the interstitial fluid (31). Other values reported are 20-35 mmHg for the plasma and 29 ± 4 and 10 ± 2 mmHg for the interstitial fluid in subcutaneous tissue and elbow, respectively (18). Therefore, in the present study the level of $\Delta\Pi$ was taken as $\Delta\Pi = 0 \pm 10$ mmHg.

The physiological value of the nondimensional parameters (*Eq. 18*) is derived by substituting the typical values cited above. Thus

$$\beta = 1.54; \qquad \lambda = 0.8; \qquad \eta = 0 \pm 0.03 \tag{22}$$

As already mentioned, the value of α may vary considerably from its typical value of 500 mmHg. Other physiological parameters may also be somewhat different from their typical values cited above. Since all the physiological parameters appear in the model (*Eqs. 19-21*), only through the values of α, β, λ, and η, in the subsequent analysis we consider a wide range of these parameters.

Relation between β and intramyocardial pump. The relation between the capillary resistance and compliance on one hand, and the intramyocardial pump mechanism on the other, can be identified by analyzing the physical meaning of the parameter β.

The capillary resistance (R) according to *Eq. 6* is

$$R = \frac{P_A - P_V}{Q} = \frac{8\mu L}{\pi a^4} \tag{23}$$

The capillary compliance (C) is

$$C = \frac{\partial V}{\partial P} = \frac{\partial}{\partial P}(\pi a^2 L) \tag{24}$$

which in view of *Eqs. 10* and *11* reduces to

$$C = \frac{2\pi L a_0^2}{\alpha} \tag{25}$$

The time constant RC of the capillary equivalent circuit thus equals

$$RC = \frac{16\mu L^2 a_0^2}{\alpha a^4} \tag{26}$$

This product, at the unloaded reference state (where $a = a_0$, $L = L_0$), is given by

$$(RC)_0 = \frac{16\mu L_0^2}{\alpha a_0^2} \tag{27}$$

The combination of the last result with *Eq. 18* gives

$$\beta = \frac{1}{3}\frac{T_0}{(RC)_0} \tag{28}$$

which means that 3β is the ratio of the cardiac cycle period T_0 to the reference time constant of the capillary $(RC)_0$. The $(RC)_0$ represents the time it takes for the flow to approach a steady state after perturbation in the external pressures P_T, P_A, and P_V. The cardiac period T_0 is the time constant of these periodic pressures. Consequently, β represents the ability of the capillary to equilibrate with the changing pressures that drive the flow.

Thus, for large values of β, changes in the boundary conditions (P_T, P_A, and P_V) would be balanced almost immediately by capillary volume changes, and the flow is essentially a quasi-steady-state one. But, when β is small, a sudden rise in these pressures (as occurs in the beginning of systole) cannot be balanced immediately by volume changes. Hence, the pressure inside the capillary would increase, driving the blood out of the capillary. The opposite occurs when the pressure drops at early diastole. This is the basis of the intramyocardial pump mechanism (37). Hence, the existence of a significant intramyocardial pump is associated with small values of β.

Preliminary assessment of relative importance of various mechanisms. The substitution of the values of the parameters (*Eq. 22*) in *Eq. 19* leads to an estimation of the relative significance of the various mechanisms to the capillary flow. Time changes in h (left-hand side of *Eq. 19*) are caused by (right-hand side of *Eq. 19* from left to right) gradient in axial flow, capillary length changes, ultrafiltration due to transmural hydrostatic pressure difference, and ultrafiltration due to transmural osmotic difference. The corresponding coefficients are $\beta = 1.54$, $\omega'(t)/\omega(t)$, (varying in time according to the input data, Fig. 1), $\lambda = 0.8$, and $\eta = 0 \pm 0.03$.

It follows that usually the most important mechanism is the axial flow gradient. Because the possible capillary length changes are not more than ±20%, they could have a significant effect only when $\omega'(t)$ is large enough (in systolic contraction and in diastolic relaxation, Fig. 1). As seen from *Eq. 19*, ultrafiltration due to transmural hydrostatic pressure difference is significant only when $\lambda(h^2 - 1)$ is not small. This happens only for distensible vessels, since for rigid vessels (large α), $h \simeq 1$ and the relative filtration effect on the flow is negligible. In all cases, the effects of transmural osmotic pressure differences are negligible.

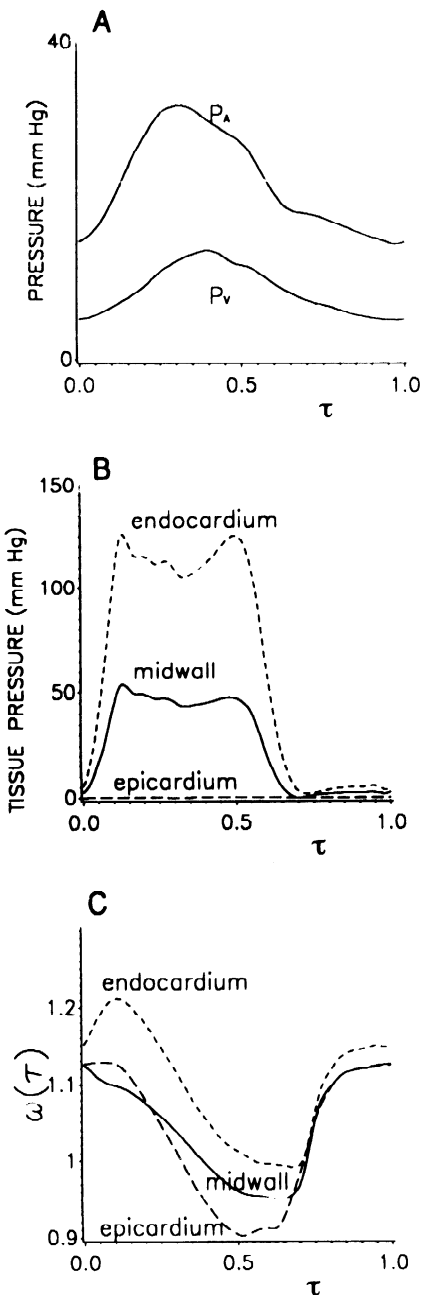

Fig. 1. Input data used in numerical simulations. *A*: time-varying pressure at arterial (P_A) and venular (P_V) ends of a subepicardial capillary. Data were digitized from Tillmanns et al. (39) and adjusted as explained in text. *B*: time-varying interstitial tissue pressure (P_T) at epicardium, midwall, and endocardium as determined from mechanical simulation of left ventricle (28). *C*: time-varying relative length change (ω) of muscle fibers at epicardium, midwall, and endocardium (results from 28). τ, time variable.

Evaluation of pressures at capillary ends. The pressures at the capillary ends (P_A and P_V) are input functions to the model, which are taken as their experimentally measured values. Tillmanns et al. (39) measured the pressures in small subepicardial arterioles and venules of the rat left ventricle. They reported peak systolic and diastolic pressures of 67 ± 12 and 45 ± 9 mmHg, respectively, for small arterioles, and 24 ± 5 and 5 ± 2 mmHg, respectively for small venules. Chilian et al. (11) reported peak systolic and diastolic pressures of 77 ± 5 and 68 ± 6 mmHg for arterioles and 11 ± 4 and 1 ± 1 mmHg for venules

of the cat left ventricle. Klassen et al. (23) reported that the pressure drops in the microcirculation and small veins in the left ventricle of a dog, during systole and diastole, were 16.4 ± 1.2 and 8.5 ± 0.8 mmHg, respectively. These pressure drops are much smaller than the ones between arterioles and venules reported by Tillmanns et al. (39) and Chilian et al. (11). The differences in the pressure data were probably caused by the different locations along the arterioles where pressures have been measured, since the pressure gradient over the arteriole level is >50 mmHg (23). The entrance pressure to the capillary should be lower than the above-cited values, since the arteriolar pressures in the studies of Tillmanns et al. (39) and Chilian et al. (11) were probably not measured near the entrance to the capillary.

In the absence of data on the pressures at the capillary ends that could serve as a basis for the present simulation, the data of Tillmanns et al. (39) for the waveform pattern in subepicardial arterioles and venules [$P_A(t)$ and $P_V(t)$] were used after scaling it linearly so that the values of the peak systolic and diastolic pressures in subepicardium were 32 and 15 mmHg for $P_A(t)$ and 13.5 and 5 mmHg for $P_V(t)$. These values are in agreement with the data of Klassen et al. (23) on the pressure gradients.

There are no data on the coronary microcirculatory pressures in the deeper layers. The values of $P_A(t)$ and $P_V(t)$ are a matter of speculation. There are two extreme cases: if the supplying and collecting vessels were rigid, then the intramyocardial tissue pressures would not have an influence on $P_A(t)$ and $P_V(t)$ at any layer of the left ventricular wall, and a reasonable approximation would be that $P_A(t)$ and $P_V(t)$ are the same for all myocardial layers. On the other hand, if these vessels were closed distensible compartments, then any change in the surrounding intramyocardial tissue pressure P_T would be followed by a similar change in arterial (P_A) and venular (P_V) pressures. This possibility was discussed by Hoffman et al. (19).

There are no conclusive data on the exact values of distensibility of the larger coronary vessels, though it is known that they are distensible (36). Yet, they are not closed compartments but rather open at both ends to inflow and outflow. Hence, changes in the intramyocardial tissue pressures P_T do affect P_A and P_V, but the extent of these effects is unknown. It can be, however, estimated, using the present model, from physiological considerations.

To present this point, it will be assumed that the levels of the pressures in the capillary inlet P_A and outlet P_V at the endocardium are the corresponding measured values at the epicardium, augmented (due to the interstitial pressure P_T) by $P_T \cdot$IPF, where IPF is the interstitial pressure factor. The value of IPF can vary between 0 (no effect) and 1 (full augmentation).

The level of IPF determines the value of the net volume of fluid exchange across the entire capillary wall due to ultrafiltration during one cardiac cycle. We denote this quantity by V_{filt}, where

$$V_{filt} = \int_{t=0}^{T_0} \int_{z=0}^{L(t)} 2\pi a q \, dz \, dt \qquad (29)$$

The net ultrafiltration volume (V_{filt}) corresponds to the fluid drainage to the lymphatic system. The latter is estimated to account for ~0.1% of the coronary flow (35). Thus the V_{filt} should be positive (i.e., in the outward direction). Moreover, the ratio of V_{filt} to the net volume of fluid that enters the capillary through the arteriolar end during one cardiac cycle (V_a) should be of the order of 0.1%, where

$$V_a = \int_{t=0}^{T_0} Q(z = 0, t) dt \qquad (30)$$

Table 1. *Values of α and corresponding values of β used in simulations*

α, mmHg	β
1,250	3.85
500	1.54
200	0.62

α, elasticity coefficient; β, nondimensional parameter. See text for more information.

As will be seen later, these considerations lead to an estimate of IPF = 0.75.

Numerical method. Discrete values of the input functions $\omega(t)$ and $P_T(t)$ for different layers in the myocardium were kindly supplied to us by Dr. E. Nevo. They are the output of a model simulation of the incompressible left ventricle in a dog (28). Data for P_A and P_V were digitized from Tillmanns et al. (39) and scaled as explained in the previous section. The continuous functions $\omega(t)$, $h_A(t)$, and $h_V(t)$, as well as their derivatives, were interpolated, using a periodic cubic spline subroutine SPER of the IMSL software package.

The parabolic *Eq. 19* was solved using the subroutine MOLCH of the IMSL software package. Because no natural initial condition exists, an initial guess was chosen as

$$h(z, t = 0) = h_A(z, 0) + z[h_V(z, 0) - h_A(z, 0)] \qquad (31)$$

which is a linear distribution of h with z between the two capillary ends. Convergence to the periodic solution in the nth cycle was checked by evaluating the maximum difference, in terms of the dimensionless radius h, between the solution of the n and the $n - 1$ cycle. Practically, for $\beta > 0.7$, it turned out that already after two cycles the difference was the order of 10^{-4}. This indicates convergence of the numeric solution after one cycle to a periodic solution.

Preliminary analysis showed that the parameter β is of predominant importance. In the following simulations the values of α and the corresponding value of β (*Eq. 18*) were taken as in Table 1, except for the results in Fig. 3.

We calculated the discharges through the arterial (Q_A) and venular (Q_V) ends of the capillary. Because of the motion of the venular end itself, Q_V is not equal to the discharge Q at the venular end as defined in *Eq. 7*, since that later quantity is measured relative to a fixed observer. Because one is interested in the net discharge (relative to the capillary end), Q_A and Q_V were determined from

$$Q_A(\tau) = -\frac{\pi a_0^4 \alpha}{48\mu L_0 \omega(\tau)} \cdot \frac{\partial}{\partial \zeta}(h^6) \quad \text{at } \zeta = 0$$
$$Q_V(\tau) = -\frac{\pi a_0^4 \alpha}{48\mu L_0 \omega(\tau)} \cdot \frac{\partial}{\partial \zeta}(h^6) \quad \text{at } \zeta = 1 \qquad (32)$$

The average inward and outward velocities (U_A and U_V) are defined as

$$U_A(\tau) = \frac{Q_A}{\pi a^2}$$
$$U_V(\tau) = \frac{Q_V}{\pi a^2} \qquad (33)$$

where, again, these are velocities relative to the corresponding capillary end.

We also define the overall inward and outward coronary discharge $\bar{Q}_{in}(\tau)$ and $\bar{Q}_{out}(\tau)$. These quantities represent the average discharge of a myocardial capillary. The averaging was done over the three different myocardial layers: subendocardium, midwall, and subepicardium.

Capillary reference volume is defined as $V_0 = \pi a_0^2 L_0$. Therefore, the relative capillary volume changes were calculated as

$$\frac{V(\tau)}{V_0} = \omega(\tau) \int_{\zeta=0}^{1} h^2 d\zeta \tag{34}$$

The average radius of the capillary is

$$\bar{a} = \frac{1}{L(t)} \int_{z=0}^{L(t)} a dz \tag{35}$$

Therefore, the average nondimensional radius is

$$\frac{\bar{a}}{a_0} = \int_{\zeta=0}^{1} h d\zeta \tag{36}$$

RESULTS

In all the following simulations, unless otherwise specified, the values used for P_A, P_V, P_T, and $\omega(t)$ are as shown in Fig. 1.

In a preliminary study, the ratio V_{filt}/V_a was calculated for three levels of α and for a range of values of the IPF. The results are presented in Fig. 2.

It is seen that for these three values of α, a choice of IPF = 0.75 provides a small positive ratio (a fraction of 1%), which is compatible with the normal physiological level of the lymphatic drainage (see *Evaluation of pressures at capillary ends*). Hence, this value was used in all subsequent calculations.

The numerical results confirm the preliminary assessment as to the insignificant effects of the ultrafiltration and osmotic pressure on the capillary flow under physiological conditions. The error due to neglecting both (i.e., $\lambda = 0$, $\eta = 0$) turns out to be <0.5%.

In the subsequent figures, the time variable is the normalized time τ (*Eq. 16*). The systolic phase is roughly τ between 0 and 0.5; the diastolic phase is between 0.5 and 1. The normalized axial position variable is ζ (*Eq. 16*), where the arterial end is at $\zeta = 0$ and the venular end is at $\zeta = 1$.

Figure 3 is a three-dimensional plot of the pressure in the capillary as a function of time and axial position for different wall distensibilities and regions across the wall. The diastolic pressure is almost the same in all cases, whereas the systolic pressure in the subendocardium increases for larger values of the distensibility α.

The pattern of the pressure distribution in the endocardium depends strongly on the value of the wall distensibility α. This term appears in the equations of the model (*Eqs. 19-21*) both in the boundary conditions and in the expressions of β and λ. The question arises whether its effect on the capillary flow (Fig. 3) is mainly through β or the boundary conditions or both (λ was already shown to have a small effect). To answer this question, the effects of β for constant α were examined in Fig. 4. The flow pattern of small vs. large β (Fig. 4) is similar to those of small vs. large α (Fig. 3), suggesting that the wall distensibility α influences the flow primarily through its effect on β.

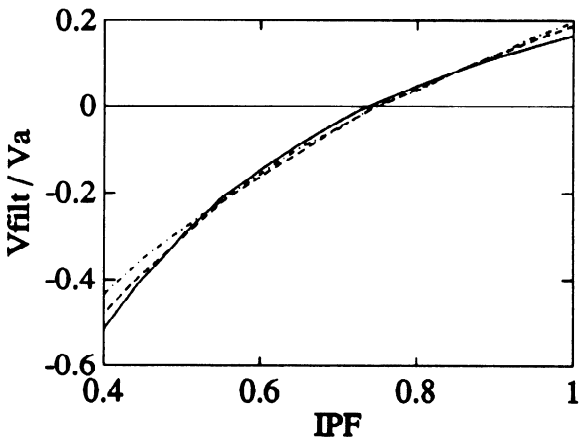

Fig. 2. Ratio of net ultrafiltration volume to net volume of arteriolar influx (V_{filt}/V_a) as a function of interstitial pressure factor (IPF) for an endocardial capillary. Three curves correspond to 3 different values of wall elasticity (α, in mmHg): 200 (solid line), 500 (dashed line), and 1,250 (dash-dot line). Input data used are as shown in Fig. 1.

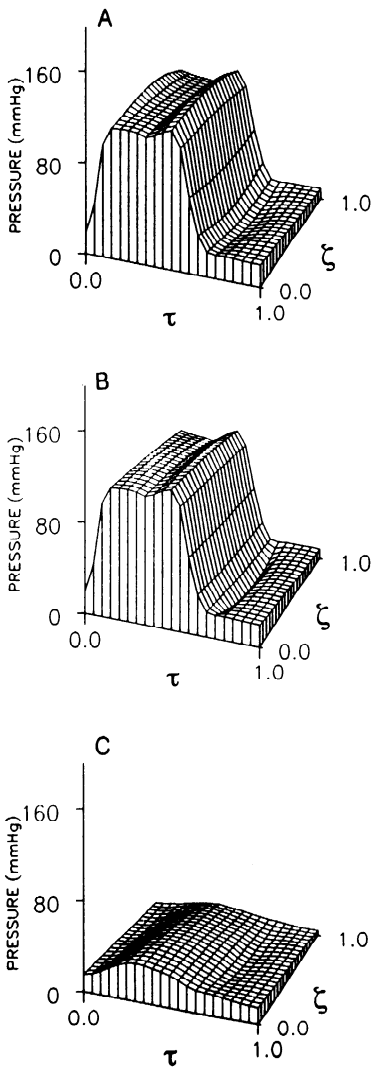

Fig. 3. Three-dimensional representation of intracapillary fluid pressure (P) as a function of time (τ) and position along capillary axis (ζ). Results are presented for various capillary distensibilities (α) and layers across the left ventricular wall. Input data used are as shown in Fig. 1. In all cases IPF = 0.75. *A*: subendocardium, α = 200 mmHg. Note that during systole pressure profile is markedly concave. This profile gives rise to a retrograde flow. *B*: subendocardium, α = 1,250 mmHg. *C*: subepicardium, α = 200 mmHg.

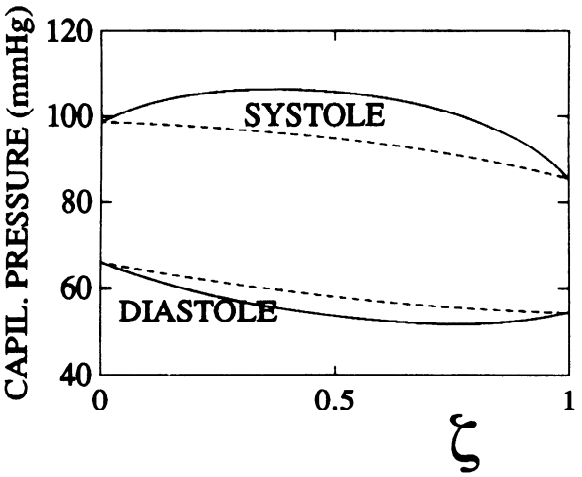

Fig. 4. Intracapillary pressure distribution along a subendocardial capillary during isovolumic contraction phase ($\tau = 0.1$ indicated as systole) and early diastole ($\tau = 0.6$ indicated as diastole) for two extreme values of the parameter β: $\beta = 0.77$ (solid lines) and $\beta = 7.7$ (dashed lines). In all cases, input data used are as shown in Fig. 1, $\alpha = 500$ mmHg and IPF = 0.75. Note existence of a concave profile at early systole and convex profile at beginning of diastole for the smaller β. This distribution results in capillary emptying during systole and filling during diastole. This is also associated with retrograde flow to the arterioles during systole and retrograde flow from the venules to the capillary at early diastole.

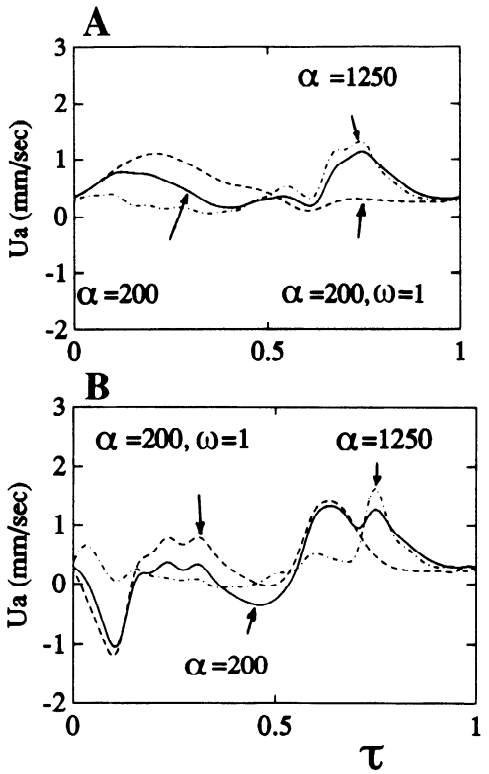

Fig. 5. Effect of α and axial stretch [$\omega(t)$] on arteriolar inflow velocity U_A. *A*: subepicardial capillary; *B*: subendocardial capillary. Three curves in each figure correspond to the following cases: $\alpha = 200$ mmHg and $\omega \equiv 1$ (no length changes), $\alpha = 200$ mmHg (and ω as in Fig. 1*C*), $\alpha = 1{,}250$ mmHg (and ω as in Fig. 1*C*). In all cases IPF = 0.75. There are considerable regional variations in the flow pattern for higher wall distensibility. Effect of length changes is more significant in epicardium.

For large values of β the pressure distribution is approximately linear. For small β, it is markedly concave in systole and convex in diastole. This pressure distribution results in an outflow from both the arterial and venular ends in early systole and an inflow from both ends during early diastole.

In the following results the effects of the wall distensibility α and the possible length changes $\omega(t)$ on the various aspects of the capillary response were investigated. This was done, since α (via β) proved to be an important flow-controlling parameter (Figs. 3 and 4), and its value may vary under different conditions. The possible capillary length change is a phenomenon that has not yet been studied in the myocardium (see *Coronary capillary mechanics and kinetics*). Hence, its influence was studied by comparing simulation results obtained using the values of length changes as shown in Fig. 1*C*, with the results obtained for the case of a fixed capillary length [$\omega(t) \equiv 1$].

An important issue in coronary circulation research is the possible existence of regional perfusion differences. For this purpose, the predicted blood velocities in the arterial and venular capillary ends were calculated (Figs. 5 and 6). The fluid velocity at the arterial end (U_A) (Fig. 5) varies significantly across the wall, especially during systole. Velocity variations in the subendocardium are greater than in subepicardium. While in the subendocardium there is a rapid retrograde flow in early systole (for small α), in the subepicardium the flow is anterograde for all values of α. Under physiological conditions, in both layers, there is a rapid filling in early diastole.

The effect of the wall distensibility α and of the capillary length changes $\omega(t)$ is markedly different for different wall layers. In subepicardium, smaller values of α result in an increase of the inflow during systole and decrease through diastole, whereas in the subendocardium this has an opposite effect: pronounced increase in the retrograde flow at early systole and a rapid filling during early diastole.

The time-varying capillary length change $\omega(t)$ has a small effect in the subendocardium but has a relatively large one in the subepicardium, where it reduces the inflow in systole while markedly increasing the inflow during diastole.

The outflow velocity (U_V) (Fig. 6) is anterograde during systole and retrograde during diastole, with much larger values in the subendocardium than in the subepicardium. As with U_A (Fig. 5), the dominant factor in the subepicardium is $\omega(t)$, whereas in the subendocardium α is of major importance.

The most reliable data available at present on coronary flow are measurements in the epicardial arteries and veins. These represent the discharges in and out of the entire myocardial wall. It is thus instructive to compare these data with the pattern of wall-averaged discharges of myocardial capillaries, as expressed by $\bar{Q}_{in}$ and $\bar{Q}_{out}$ (see *Phasic flow patterns*).

The effect of α and $\omega(t)$ on $\bar{Q}_{in}$ is shown in Fig. 7. A similar pattern can be observed in all cases: small inflow during early systole and rapid filling in early diastole. A smaller value of α results in larger systolic-diastolic flow variations, with retrograde flow in early systole. $\omega(t)$ tends to decrease the inflow during late systole and to increase it during late diastole.

The opposite behavior is seen for $\bar{Q}_{out}$ (Fig. 8): there is

a rapid venular emptying during early systole and retrograde filling during diastole. Again, lower values of α increase the systolic-diastolic flow differences. $\omega(t)$ increases both the systolic emptying and the diastolic retrograde filling.

Capillary capacitance and the possible existence of an intramyocardial pump mechanism are closely related to capillary volume changes. From Fig. 9 it is seen that there are substantial volume changes that are larger in the subendocardium (up to 30%) compared with the subepicardium (20%). The volume decreases during systole and increases during diastole. $\omega(t)$ has a predominant effect in the subepicardium, while in the subendocardium α is the most significant factor.

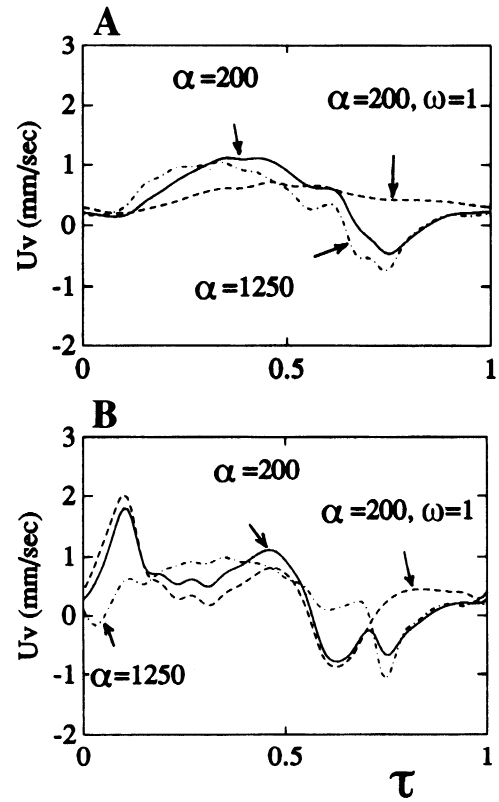

Fig. 6. Time-varying outflow velocity into venule (U_V) under same conditions as in Fig. 5.

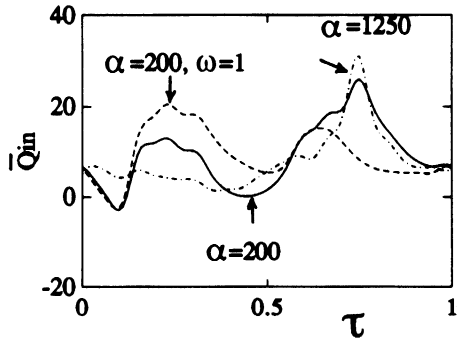

Fig. 7. Time-varying entrance discharge ($\bar{Q}_{in}$) averaged across left ventricular wall (average of subendocardium, midwall, and subepicardium). Three curves in each figure correspond to the following cases: α = 200 mmHg and $\omega \equiv 1$ (no length changes), α = 200 mmHg (and ω as in Fig. 1*C*), α = 1,250 mmHg (and ω as in Fig. 1*C*). IPF = 0.75. Discharge units are $cm^3 \cdot s^{-1} \cdot 10^{-9}$. Note rapid filling during diastole, except when there are no length changes.

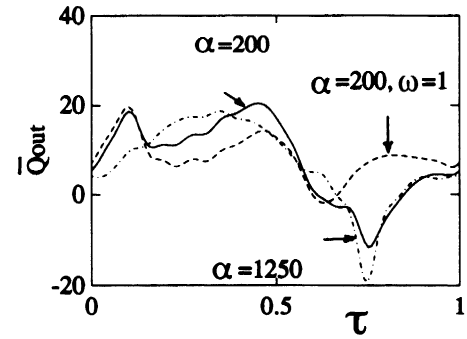

Fig. 8. Time-varying exit discharge $\bar{Q}_{out}$ under same conditions as in Fig. 7. There is a retrograde diastolic flow and increased systolic anterograde flow except when there are no length changes.

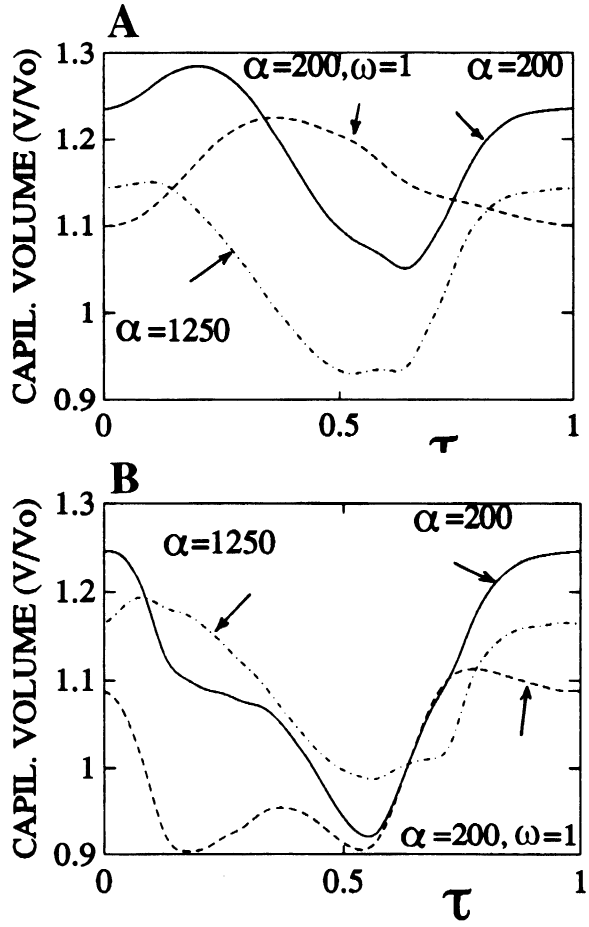

Fig. 9. Relative capillary volume change during cardiac cycle as affected by capillary wall distensibility α and capillary length changes ω for IPF = 0.75. *A*: subepicardial capillary; *B*: subendocardial capillary. Three curves in each figure correspond to the following cases: α = 200 mmHg and $\omega \equiv 1$ (no length changes), α = 200 mmHg (and ω as in Fig. 1*C*), α = 1,250 mmHg (and ω as in Fig. 1*C*). Note regional differences and considerable volume changes for all values of α. These volume changes result in a pumping effect.

The variations of the (length-averaged) capillary radius with time are presented in Fig. 10. The variations are larger for smaller α (10% in endocardium; 5% in epicardium), whereas for large α the variations are <2%. Opposite behaviors are observed for different regions: subepicardial capillaries radii tend to increase during systole and decrease in diastole, while the opposite is true for subendocardial capillaries.

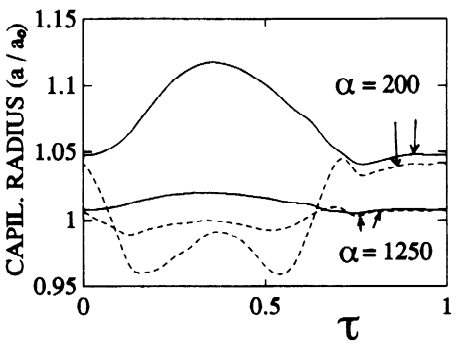

Fig. 10. Time-varying capillary radius as affected by location across left ventricular wall and capillary wall distensibility. Diameter is averaged along capillary axis and normalized to reference radius (a_0). Solid and dashed lines represent subepicardial and subendocardial capillaries, respectively.

DISCUSSION

The distributive analysis presented here allows one to gain understanding of the complex interactions among multiple factors affecting the coronary capillary flow and to assess quantitatively the relative importance of different determinants of that flow. This methodology provides a theoretical framework for the inclusion of additional factors such as pathological processes, capillary branching, and more accurate representation of the collagen fiber interaction with the capillary.

Subepicardial microcirculatory flow. Most of the available data relates to the flow in the subepicardium. Tillmanns et al. (38) and Ashikawa et al. (1) measured the red blood cell velocities in subepicardial arterioles, capillaries, and venules. There are substantial differences between the results of these two studies. Ashikawa et al. (1) observed a similar pattern of flow in all microvessels with retrograde flow in early systole, whereas Tillmanns et al. (38) did not observe retrograde flow, and the flow pattern in arterioles was opposite to those of capillaries and venules: reduced systolic flow in arterioles and increased systolic flow in capillaries and venules.

The difference between the experimental results of the above two studies may originate from the different species (turtle vs. dog) but may also be due to the fact that measurements were made of absolute red blood cell velocities (measured relative to a fixed observer). These velocities are the superposition of the red blood cell velocity relative to the capillary wall, the wall axial velocity (as a result of the length changes of the capillary), and the lateral motion of the whole microvessel together with the contracting myocardium. The motion of the myocardium depends strongly on the tissue fixation conditions, which were different in these two studies. In the present study, on the other hand, the velocities U_A and U_V were evaluated as net velocities relative to the entrance and exit of the capillary, respectively, since these velocities determine the blood supply to the tissue.

In addition, the different fixation conditions might have introduced artificial restraint and thus influenced the freedom of length changes of the myocytes and adjacent capillaries. Because velocities in the subepicardium are strongly sensitive to these length changes (Figs. 5*A* and 6*A*), this restraining may be another reason for the differences between the above observations.

The present model agrees with the observations of Tillmanns et al. (38). Still, the above discussion indicates that this similarity should be regarded with caution.

Phasic flow patterns. It is instructive to compare data of epicardial arterial flow and venular return with the model's predictions of the wall-averaged capillaries discharges $\bar{Q}_{in}$ and $\bar{Q}_{out}$. Although we are comparing two different quantities, since the overall coronary response (as measured in the epicardial vessels) is the combined contribution of the entire intramyocardial system, the comparison is important for the following reason. Because the capillaries occupy a large fraction of the coronary vasculature volume, if the capillary shows patterns of behavior that are similar to those of the measured epicardial phasic flows, then this would indicate that capillaries play a substantial role in the overall coronary response. On the other hand, if the patterns are qualitatively different, then the conclusion would be that larger vessels are predominant and that the role of capillaries is less important.

Systolic retrograde flow in the coronary arteries was observed in several studies (e.g., 12, 21, 37). The retrograde flow occurs mainly in early systole, followed by moderate anterograde flow in midsystole, a leveling or even a decline in late systole, followed by rapid filling in early diastole (12, 21). Most of the coronary arterial flow occurs during diastole.

The model predictions for the average capillary inward discharge $\bar{Q}_{in}$ are compatible with these patterns of behavior, as can be seen in Fig. 7. Moreover, the model predicts that during systole, the pressures in the endocardial arterioles and venules would be much higher than in the epicardial ones. This also suggests a systolic retrograde flow in the arterioles.

Several studies have shown that there is an approximately 180° phase-shift between arterial and venular flow in the extramural vessels (e.g., 22). This observation is compatible with the model's prediction when comparing $\bar{Q}_{in}$ and $\bar{Q}_{out}$ (Figs. 7 and 8).

Another observation is that in systole there is a peak of flow in the extramural veins (e.g., 21). This is in accordance with the model's prediction showing peak total venular outflow ($\bar{Q}_{out}$) at systole.

The flow to the subendocardial layers slows down during systole (e.g., 17), as predicted by the model (Fig. 4*B*).

Wall distensibility. α turns out to be the key parameter that determines the pattern of the flow in the endocardium (mainly through the nondimensional parameter β). In the epicardium, the flow pattern is less influenced by the value of α. This higher sensitivity to α in the subendocardium is explained by the higher interstitial pressure variations in time that exist there. For large α (hence large β), the flow can be approximated as a quasi-steady flow. Small values of α (and β) give rise to an intramyocardial pumping phenomena (i.e. alternate anterograde and retrograde flows) associated with considerable cyclic changes of capillaries diameter and volume. Thus, from comparison with the known coronary flow characteristics, it seems more likely that the actual value of α should be small (in the range of 200–500 mmHg).

Capillary length changes. The results of Poole et al. (30) suggest that elastic length changes may occur in the coronary capillaries, as was observed in skeletal muscle for sarcomere length above 2.1 μm. If such changes exist, then they are the dominant mechanism in the subepicardium, since interstitial pressures are small. From Fig. 1*C* and the assumption expressed by *Eq. 3*, it follows that capillary length decreases in systole by 20–25% relative to diastole. This has a direct effect on the volume of fluid contained in the capillary. In systole, the shortening of the capillary results in an emptying through both ends. This increases the outflow at the venular end and decreases the inflow (or even gives rise to retrograde flow) in the arterial end. In diastole, the capillary lengthening results in pumping of fluid into the capillary. As a result, inflow through the arterial end becomes stronger and outflow at the venular end is reduced (or retrograde flow increases). Hence, this discharge effect due to the length changes is in phase with the intramyocardial pumping, thus increasing its strength.

Interstitial pressure factor. In *Evaluation of pressures at capillary ends*, the value of IPF was estimated to be ~0.75 from consideration of the lymphatic drainage (Fig. 2). The ratio of filtration to capillary discharge increases monotonically with IPF, since higher IPF leads to a rise in the capillary pressure and hence to a larger outward ultrafiltration.

Intramyocardial tissue pressure P_T. Because the level of intramyocardial pressure in the outer layers is small, it is mainly in the deeper layers where it influences the flow. The intramyocardial pressure controls the capillary flow through two distinct mechanisms. First, it applies stress on the supplying arteriole and collecting venules, which causes P_A and P_V to increase by IPF$\cdot P_T$ (see *Evaluation of pressures at capillary ends*). Hence, the pressure inside the capillary P would also increase by IPF$\cdot P_T$ (*Eq. 20*). The second effect of P_T is through the stresses it exerts on the capillary wall. The net result of these two mechanisms is an effective interstitial pressure of $(1 - \text{IPF}) \cdot P_T$.

It was already shown that large values of β correspond to the ability of the capillary to undergo rapid volume changes. Because P_T is practically uniform along the capillary, its effect would be merely to compress the capillary without changing the quasi-steady pattern of the flow. For small β, a rise in P_T in early systole cannot be balanced immediately by fluid outflow. Hence, the pressure in the capillary would rise accordingly. The pressure attains maximum level at midcapillary, and the pressure gradients cause emptying of the fluid at both ends. In early diastole, the sudden decline in P_T cannot be balanced by rapid fluid filling. Hence, the pressure in the capillary falls, so that fluid is pumped into the capillary. This is the basis of the intramyocardial pump phenomena.

Ultrafiltration and osmotic pressure effects. The present numerical and dimensional analysis shows that both factors have no significant effect on the flow in the range of physiological parameters. Filtration due to transmural hydrostatic pressure difference could, in principle, have a more significant influence, as revealed by *Eq. 19*. The term representing filtration due to transmural hydrostatic pressure differences is $\lambda(h^2 - 1)$. Since λ is of order 1, then this term becomes significant if the capillary radius changes significantly during the cardiac cycle, so that $|h^2 - 1| \gg 0$. Large variations of the radius are likely to occur if the wall is distensible (i.e., for small α). The present analysis suggests that even for the smaller values of α used (200 mmHg), ultrafiltration does not become a significant factor in the capillary flow.

Regional differences. The present model predicts different flow patterns in the subendocardium vs. subepicardium. This results mainly from the difference in the intramyocardial pressure P_T between these layers. In all layers, the pressure gradient between P_A and P_V is the driving force for the basic flow. But whereas in the subepicardium this is superimposed by the effects of capillary length change, in the subendocardium the varying intramyocardial tissue pressures P_T is the most significant additional mechanism. The net result is that the capillary contribution to the overall pumping effect is considerably larger in the subendocardium.

Capillary volume changes. The model predicts capillary diastolic/systolic volume changes of up to 20% in the subepicardium and 35% in the subendocardium. These changes are the result of the capillary length change (which accounts for a volume change of ~20%) and also of the radius changes (Fig. 9). Levy et al. (26) reported that capillary volume decreases by 50% from diastole to systole. Hoffman and Spaan (20) suggest that because of the techniques used in that study, the above results may have somewhat overestimated the dynamic, in vivo volume changes. With this taken into consideration, the predictions of the model are compatible with the actual capillary volume changes.

Tillmanns et al. (38) report that capillary radius in the subepicardium decreases by 34% between diastole and systole. The results of Ashikawa et al. (1) and Poole et al. (30) suggest that the changes in radius are very small. The present analysis predicts a decrease of radius in endocardial capillaries during systole but an increase in the systolic radius for subepicardial capillaries with high extensibility (low α). This radius increase of subepicardial capillaries during systole is the result of increased systolic pressures P_A and P_V at both ends of the distensible capillary, while the surrounding intramyocardial pressure P_T is negligible there. Stiffer subepicardial capillaries show little diastolic-systolic radius change, a result compatible with some of the above data.

Capillary collapse. The assumption that coronary microvessels collapse is based on the existence of very large pressure differences across the capillary wall as a result of high tissue pressure in the endocardium. The present analysis shows, however, that a rise in the tissue pressure is followed by rise in the capillary pressure. Thus the effective pressure difference across the capillary wall as a result of the tissue pressure is ~25% of the tissue pressure value. This suggests that capillary collapse is less likely to occur.

The present numerical simulations did not demonstrate collapse in the capillaries, although higher capillary distensibility may in principle give rise to partial or total collapse. A more detailed study is needed of capillary wall mechanics and of the effect of the collagen struts

throughout the cardiac cycle before a realistic analysis of the possibility of collapse can be carried out. There are, however, other observations in the literature that shed light on this issue. Because during systole the collagen struts were found to be taut (6), it does not seem reasonable that collapse of capillaries could occur during systole. During diastole the interstitial pressure is low so that diastolic capillary collapse seems unreasonable as well.

Model analysis. The present work deals with a model of a single straight capillary with uniform properties. As with any model, detailed comparison between theory and experiment should be done with caution. The main role of a model is to assess the role and importance of various properties and/or parameters, as discussed above in detail. This holds true also when comparing results of a single capillary with experimental results from a network. The assumed capillary geometry of a network of isolated parallel long vessels is obviously only an approximate representation of the essence of the coronary capillary system. A more realistic picture should consider also the cross-connections between neighboring capillaries (at distances of ~ 75 μm from each other) and some degree of branching. Analysis of such a network should regard the time-varying pressures at the network junctions as unknown functions, resulting in a system of nonlinear equations. A solution is possible if realistic data become available on the network geometry, including its multiple hydraulic connections with the supplying arterioles and collecting venules. In addition, data on the branching of capillaries and on the nonuniformity are required. In the framework of such a network, the present model of a long single vessel is applicable for vessel segments that are long (e.g., portion of capillaries between cross-connections). The three-dimensional aspect of the capillary system can be incorporated just as well by considering neighboring vessels at adjacent myocardial layers, which are loaded by slightly different tissue pressure and interconnected by translayer cross-connections.

Yet despite the present model limitations, the analysis provides results for the combined capillary flow that exhibit similar characteristics to the measured phasic coronary flow. This suggests that the present approach is generally correct and that some important flow-controlling mechanisms have been correctly dealt with.

Conclusions. The following conclusions are made.

First, the analysis shows the existence of regional differences in the coronary flow. In the epicardium, the capillary flow is essentially quasi-steady, driven by the pressure difference between the capillary ends. In the endocardium, the capillary flow pattern is more complex and is reminiscent of an intramyocardial pump.

Second, the interstitial pressure is a key factor in controlling capillary flow in deeper left ventricular layers. The extent of its influence is determined by the wall distensibility. In particular, intramyocardial pumping effects are associated mainly with high capillary distensibility (small α). Because there is a possibility of variation in the elastic response of the wall during the cardiac cycle, it is important that in future studies this topic will be studied in detail based on realistic microstructural features.

Third, although the speculated capillary cyclic length changes may occur in all myocardial layers, their effect turned out to be most significant in the outer layers of the left ventricular wall where intramyocardial pressure is low. The length changes result in an additional pumping effect, which although smaller than the one associated with wall distensibility, acts in phase with it.

Finally, the pressure inside a subendocardial microvessel is augmented by $\sim 75\%$ of the interstitial tissue pressure around it. This suggests smaller pressure differences across its wall and a flow from the inner layers to the superficial ones during systole, which results in overall retrograde systolic flow.

Current address for G. Fibich: 251 Mercer St., Courant Institute, New York, NY 10012.

Address for reprint requests: Y. Lanir, Cardiac System Research Ctr., Dept. of Biomedical Engineering, Technion-Israel Institute of Technology, Haifa 32000, Israel.

Received 19 February 1992; accepted in final form 16 June 1993.

REFERENCES

1. **Ashikawa, K., H. Kanatsuka, T. Suzuki, and T. Takishima.** Phasic blood flow velocity pattern in epimyocardial microvessels in the beating canine left ventricle. *Circ. Res.* 59: 704-711, 1986.
2. **Baldwin, A., and R. W. Gore.** Simultaneous measurement of capillary distensibility and hydraulic conductance. *Microvasc. Res.* 38: 1-22, 1989.
3. **Bassingthwaighte, J. B., T. Yipintsoi, and R. B. Harvey.** Microvasculature of the dog left ventricle myocardium. *Microvasc. Res.* 7: 229-249, 1974.
4. **Berne, R. M., and R. Rubio.** Coronary circulation. In: *Handbook of Physiology. The Cardiovascular System. The Heart.* Bethesda, MD: Am. Physiol. Soc., 1979, sect. 2, vol. I, chapt. 25, p. 873-952.
5. **Beyar, R., and S. Sideman.** Time-dependent coronary blood flow distribution in left ventricular wall. *Am. J. Physiol.* 252 (*Heart Circ. Physiol.* 21): H417-H433, 1987.
6. **Borg, T. K., and J. B. Caulfield.** The collagen matrix of the heart. *Federation Proc.* 40: 2037-2041, 1981.
7. **Boseck, G. L.** *Transcapillary Fluid Exchange in Rat Spinotrapezius Muscle* (PhD thesis). La Jolla, CA: Univ. of California at San Diego, 1983.
8. **Caulfield, J. B., and T. K. Borg.** The collagen network of the heart. *Lab. Invest.* 40: 364-372, 1979.
9. **Chadwick, R. S.** Slow viscous flow inside a torus. The resistance of small tortuous blood vessels. *Q. Appl. Math.* 43: 317-323, 1985.
10. **Chadwick, R. S., A. Tedgui, J. B. Michel, J. Ohayon, and B. I. Levy.** Phasic regional myocardial inflow and outflow: comparison of theory and experiments. *Am. J. Physiol.* 258 (*Heart Circ. Physiol.* 27): H1687-H1698, 1990.
11. **Chilian, W. M., S. M. Layne, E. C. Klausner, C. L. Eastham, and M. L. Marcus.** Redistribution of coronary microvascular resistance produced by dipyridamole. *Am. J. Physiol.* 256 (*Heart Circ. Physiol.* 25): H383-H390, 1989.
12. **Chilian, W. M., and M. L. Marcus.** Phasic coronary blood flow velocity in intramural and epicardial coronary arteries. *Circ. Res.* 50: 775-781, 1982.
13. **Dinnar, U.** Interaction between intramyocardial pressure and transcapillary exchange: a possible control of coronary circulation. In: *Simulation and Control of the Cardiac System,* edited by S. Sideman and R. Beyar. CRC, 1987, p. 109-130.
14. **Downey, J. M., and E. S. Kirk.** Inhibition of coronary blood flow by a vascular waterfall mechanism. *Circ. Res.* 36: 753-760, 1975.
15. **Ellis, C. G., O. Mathieu-Costello, R. F. Potter, I. C. MacDonald, and A. C. Groom.** Effect of sarcomere length on total capillary length in skeletal muscle: in vivo evidence for longitudinal stretching of capillaries. *Microvasc. Res.* 40: 63-72, 1990.
16. **Feigl, E. O.** Coronary physiology. *Physiol. Rev.* 63: 1-204, 1983.
17. **Hanley, F. L., L. M. Messina, M. T. Gratten, and J. I. E. Hoffman.** The effects of coronary inflow pressure on coronary

vasculature resistance in the isolated dog heart. *Circ. Res.* 54: 760–772, 1984.

18. **Hargens, A. R.** Interstitial fluid pressure and lymph flow. In: *Handbook of Bioengineering*, edited by R. Skalak and S. Chien. New York: McGraw-Hill, 1987, p. 19.1–19.25.
19. **Hoffman, J. I. E., R. W. Baer, F. L. Mandey, and L. M. Messina.** Regulation of transmural myocardial blood flow. *ASME Trans. J. Biomech. Eng.* 107: 3–9, 1985.
20. **Hoffman, J. I. E., and J. A. E. Spaan.** Pressure flow relations in coronary circulation. *Physiol. Rev.* 70: 331–390, 1990.
21. **Kajiya, F., G. Tomonaga, K. Tsujioka, Y. Ogasawara, and H. Nishihara.** Evaluation of local blood flow velocity in proximal and distal coronary arteries by laser doppler method. *ASME Trans. J. Biomech. Eng.* 107: 10–15, 1985.
22. **Kajiya, F., K. Tsujioka, Y. Ogasawara, O. Hiramatsu, Y. Wada, M. Goto, and M. Yanaka.** Analysis of the characteristics of the flow velocity waveform in left atrial small arteries and veins in the dog. *Circ. Res.* 65: 1172–1181, 1989.
23. **Klassen, G. A., J. A. Armour, and J. B. Garner.** Coronary circulatory pressure gradients. *Can. J. Physiol. Pharmacol.* 65: 520–531, 1987.
24. **Klocke, F. J., R. E. Mates, J. M. Canty, Jr., and A. K. Ellis.** Coronary pressure flow relationship-controversial issues and probable implications. *Circ. Res.* 56: 310–323, 1985.
25. **Krams, R., P. Sipkema, and N. Westerhof.** Coronary oscillatory flow amplitude is more affected by perfusion pressure than ventricular pressure. *Am. J. Physiol.* 258 (*Heart Circ. Physiol.* 27): H1889–H1898, 1990.
26. **Levy, B. I., J. L. Samuel, A. Tedgui, V. Kotelianski, F. Marotte, P. Poitevin, and R. S. Chadwick.** Intramyocardial blood volume in the left ventricle of rat arrested hearts. In: *Cardiovascular Dynamics and Models*, edited by P. Brun, R. S. Chadwick, and B. I. Levy. Paris: INSERM, 1988, p. 65–71. (Colloque INSERM 183)
27. **Lipowsky, H. H., S. Kovalcheck, and B. W. Zweifach.** The distribution of blood rheological parameters in the microcirculation of cat mesentery. *Circ. Res.* 43: 738–749, 1978.
28. **Nevo, E., and Y. Lanir.** Structural finite deformation model of the left ventricle during diastole and systole. *ASME Trans. J. Biomech. Eng.* 3: 342–348, 1989.
29. **Ono, T., Y. Shimohara, K. Okada, and S. Irino.** Scanning electron microscopic studies on microvascular architecture on human coronary vessels by corrosion casts: normal and focal necrosis. *Scanning Electron Microsc.* 1: 263–270, 1986.
30. **Poole, D. C., S. Batra, O. Mathieu-Costello, and K. Rakusan.** Capillary geometrical changes with fiber shortening in rat myocardium. *Circ. Res.* 70: 697–706, 1992.
31. **Ruch, T. C., and H. D. Patton.** *Physiology and Biophysics.* Philadelphia, PA: Saunders, 1966.
32. **Schmid-Schönbein, G. W., S. Y. Lee, and D. Sutton.** Dynamic viscous flow in distensible vessels of skeletal muscle microcirculation: application to pressure and flow transients. *Biorheology* 26: 215–227, 1989.
33. **Skalak, T. C., and G. W. Schmid-Schönbein.** Viscoelastic properties of microvessels in rat spinotrapezius muscle. *ASME Trans. J. Biomech. Eng.* 108: 193–200, 1986.
34. **Smaje, L. H., and G. T. G. Swayne.** The effects of compliance on measurement of hydraulic conductivity in microvessels. *Biorheology* 21: 171–179, 1984.
35. **Solti, F., and H. Jellinek.** *Cardiac Lymph Circulation and Cardiac Disorders.* Budapest: Akademiai Kiado, 1989.
36. **Spaan, J. A. E.** Coronary diastolic pressure-flow relation and zero flow pressure explained on the basis of intramyocardial compliance. *Circ. Res.* 56: 293–309, 1985.
37. **Spaan, J. A. E., N. Breuls, and J. Laird.** Diastolic systolic coronary flow differences are caused by intramyocardial pump action in the anesthetized dog. *Circ. Res.* 49: 584–593, 1981.
38. **Tillmanns, H., S. Ileda, H. Hansen, S. Jonnalagedda, M. Sarma, J. Fauvel, and R. Bing.** Microcirculation in the ventricle of the dog and turtle. *Circ. Res.* 34: 561–568, 1974.
39. **Tillmanns, H., M. Steinhausen, H. Leinberger, H. Thederan, and W. Kubler.** Pressure measurements in the terminal vascular bed of the epimyocardium of rats and cats. *Circ. Res.* 49: 1202–1211, 1981.